Organic & Biomolecular Chemistry

ROYAL SOCIETY OF CHEMISTRY

PAPER

View Article Online
View Journal | View Issue

Cite this: *Org. Biomol. Chem.*, 2021, **19**, 911

A near-infrared fluorescent probe that can image endogenous hydrogen polysulfides *in vivo* in tumour-bearing mice†

Ling Zhang, *[a,b] Huizhen Liu,[a] Chunli Wu,[a] Youguang Zheng,[a] Xiaoning Kai[a] and Yunsheng Xue*[a]

Received 12th November 2020,
Accepted 23rd December 2020

DOI: 10.1039/d0ob02253e

rsc.li/obc

Hydrogen polysulfides (H_2S_n, $n > 1$), which are important reactive sulfur species, play crucial roles in H_2S-related bioactivities, including antioxidation, cytoprotection, activation of ion channels, transcription factor functions and tumour suppression. Monitoring H_2S_n *in vivo* is of significant interest for exploring the physiological roles of H_2S_n and the exact mechanisms of H_2S_n-related diseases. Herein, we conceive a novel near-infrared fluorescent probe, NIR-CPS, that is used to detect H_2S_n in living cells and *in vivo*. With the advantages of high sensitivity, good selectivity and a remarkably large Stokes shift (100 nm), NIR-CPS was successfully applied in visualizing H_2S_n in living cells and mice. More importantly, NIR-CPS monitored H_2S_n stimulated by lipopolysaccharide in tumour-bearing mice. These results demonstrate that the NIR-CPS probe is a potentially powerful tool for the detection of H_2S_n *in vivo*, thus providing a valuable approach in H_2S_n-related medical research.

Introduction

Reactive sulfur species (RSS), which are a family of sulfur-containing molecules, play essential roles in cell transduction, redox homeostasis, and metabolic regulation.[1–3] Representative RSSs include thiols, hydrogen sulfide (H_2S), persulfides (RSSH), polysulfides (RSS_nSR), *S*-nitrosothiols (SNO) and sulfenic acids (SOH), as well as inorganic sulfur derivatives.[4] Among them, H_2S is the most attractive, as it has been demonstrated to be the third gaseous signalling molecule.[5] H_2S has diverse biological functions, including vasodilation, neurotransmission, insulin secretion, inflammation regulation, apoptosis and ischaemia/reperfusion-induced injury.[6–8]

H_2S_n (hydrogen polysulfides) and H_2S always coexist in biological systems. H_2S_n can be derived from H_2S in the presence of reactive oxygen species (ROS),[9] and H_2S_n can also degrade into a precursor of H_2S. Recent research suggests that H_2S_n may be the actual signal transduction molecule in H_2S-related bioactivities,[10–15] although this remains controversial. *S*-Sulfhydration of cysteine residues (SH → SSH) was originally attributed to H_2S. Recent results revealed that H_2S_n is more effective than H_2S in protein *S*-sulfhydration.[9,11–14,16–18] H_2S_n has been implicated in a number of physiological and pathological processes. H_2S_n was found to activate tumour suppressor protein, lipid phosphatase and the tensin homologue (PTEN) by *S*-sulfhydration.[14] Additionally, H_2S_n exhibited higher potency than H_2S in inducing Ca^{2+} influx in astrocytes by activating transient receptor potential ankyrin 1 (TRAP1) channels.[18–20] H_2S_n can effectively relax vascular smooth muscle by activating protein kinase G1a (PKG1α).[21] H_2S_n also exhibited crucial antioxidant activities in the cellular redox milieu. This is due to H_2S_n mediating the activation of Nrf2 signalling, subsequently causing the elevation of intracellular GSH levels and the expression of HO-1 (a Nrf2-regulatory gene).[22] These results demonstrate that H_2S_n possesses diverse biological functions, including antioxidation, cytoprotection, activation of ion channels, transcription factor functions and tumour suppression. In addition, H_2S_n appears to be involved in several diseases, including cancers, ethylmalonic encephalopathy, Parkinson's disease (PD), and Huntington's disease (HD).[23] However, compared with other biothiols (RSH), the fundamental chemical biology of H_2S_n has yet to be further elucidated.

To better explore the physiological and pathologic roles of H_2S_n, a sensitive and effective detection method for H_2S_n is urgently needed. The traditional methods for detecting poly-

[a]*Jiangsu Key Laboratory of New Drug Research and Clinical Pharmacy, Jiangsu Center for the Collaboration and Innovation of Cancer Biotherapy, School of Pharmacy, Xuzhou Medical University, Xuzhou, 221002, P. R. China. E-mail: zhamgling1999@163.com, xzmcysxue@sina.com*

[b]*NHC Key Laboratory of Nuclear Medicine, Jiangsu Key Laboratory of Molecular Nuclear Medicine, Jiangsu Institute of Nuclear Medicine, Wuxi, 214063, P. R. China*

†Electronic supplementary information (ESI) available: Additional materials, methods and figures, including fluorescence spectra, cell imaging, live mouse imaging, NMR and HRMS spectra, and a detailed protocol for synthesis. See DOI: 10.1039/d0ob02253e

sulfides, such as UV-Vis spectroscopy and mono-bromobimane (MBB)-based detection, are limited by poor sensitivity and destructiveness.[14,18,24] Fluorescence assays are powerful tools for monitoring H_2S_n, owing to their high sensitivity, excellent spatiotemporal resolution ability, and nondestructiveness.[25,26] The first H_2S_n fluorescent probe was developed by the Xian group,[27] and several H_2S_n probes have been subsequently reported. To date, various types of probes have been reported for detecting H_2S_n, including ratiometric probes, two-photon probes, near-infrared probes, dual response probes, mitochondria-targetable probes, lysosome-targetable probes, and endoplasmic reticulum-targetable probes.[4,28–46] Several sensing strategies have been used in the design of H_2S_n-selective fluorescent probes by taking advantage of the strong nucleophilicity and reduction ability of H_2S_n, including H_2S_n-mediated aromatic substitution cyclization, the H_2S_n-mediated ring-opening reaction of aziridine and H_2S_n-mediated reduction of the nitro group.[4] Nevertheless, the selective detection of H_2S_n is still challenging due to the interference of other biothiols, such as H_2S, GSH, Cys, Hcy, and thiol-containing proteins, that have similar chemical properties to H_2S_n. Moreover, as the physiological levels of endogenous H_2S_n are low in cells/plasma/tissues, the sensitivity of the current H_2S_n probes could still be improved. Additionally, probes for the detection of endogenous H_2S_n *in vivo*, especially in pathological conditions, such as cancers, are still sparse. Therefore, it is important to develop an NIR fluorescent probe for imaging H_2S_n with desirable characteristics, especially high sensitivity and the ability to monitor endogenous H_2S_n *in vivo* in tumour-bearing mice.

Compared with H_2S_n probes with emission in the visible region, near-infrared (NIR) probes are more desirable for detection *in vivo* due to deep tissue penetration, minimal optical damage to biological samples, and minimal interference from background autofluorescence.[47,48] Herein, we conceived a novel NIR fluorescent probe, NIR-CPS, for H_2S_n detection *in vivo*. The NIR-CPS probe could provide good selectivity, high sensitivity (a detection limit of 18 nM) and a remarkably large Stokes shift (100 nm). NIR-CPS was utilized to image endogenous H_2S_n in living cells and mice. Significantly, the application of NIR-CPS in tumour-bearing mice suggested that the probe could image intratumoural H_2S_n *in vivo*, highlighting its great potential for exploring the anticancer mechanism of polysulfide.

Results and discussion

Design and synthesis of NIR-CPS

In the design of an NIR probe for H_2S_n, the Changsha analogue dye icyanoisophorone was selected as a fluorophore due to its NIR emission and large Stokes shift.[49–51] *p*-Nitrofluorobenzoate served as the H_2S_n recognition group as well as a fluorescence quencher.[27] H_2S_n has been proven to be both an effective nucleophile and electrophile.[4] We anticipated that the fluorescence of a fluorophore can be quenched by the nitrofluorobenzoate group. The fluorobenzoate group would trap H_2S_n by replacing the F atom, forming the persulfide intermediate with the –SSH group; then, –SH, as a nucleophile, continues to react with the carbonyl group, which further promotes cyclization to release the fluorophore NIR-OH with NIR fluorescence emission (Scheme S1†). The NIR-CPS probe was prepared by the reaction of compound 1 with intermediate 2 in the presence of piperidine (Scheme S2†). The structure of the NIR-CPS probe was characterized by NMR spectroscopy and mass spectrometry (Fig. S14–S22†).

Response mechanism of NIR-CPS

To assess the sensing performance of NIR-CPS, the product of the NIR-CPS reaction with H_2S_n was purified and analysed. The fluorescence and UV-vis analyses of the mixture solution show the same emission spectra and absorption spectra as the compound NIR-OH (Fig. S1†). The results of NMR spectroscopy and mass spectrometry confirmed the mechanism of this reaction as illustrated in Scheme 1.

Fluorescence response of NIR-CPS to H_2S_n *in vitro*

The absorption and fluorescence sensing of NIR-CPS towards H_2S_n were both tested under simulated physiological conditions. With the addition of Na_2S_4 (0–300 μM) to a solution containing NIR-CPS, the maximum absorption changed from 552 nm to 570 nm (Fig. S1†). In the absence of Na_2S_4, a negligible fluorescence signal was observed (Fig. 1). After treatment of NIR-CPS with different concentrations of Na_2S_4 (0–300 μM), a significant fluorescence emission peak at 670 nm gradually increased (20-fold) and reached a plateau at 100 μM Na_2S_4 (Fig. 1). Moreover, there was a linear relationship between the fluorescence intensity and the concentrations of Na_2S_4 from 0–20 μM (Fig. 1). The detection limit was determined to be as low as 18 nM in PBS buffer, which was lower than most previously reported H_2S_n probes (Table S1†). It should be noted that the NIR-CPS probe has a remarkably large Stokes shift (100 nm) (Fig. S1†), which can eliminate the measurement interference and self-quenching induced by the excitation and scattered light. These results indicate the feasibility of NIR-CPS for the quantitative and qualitative detection of H_2S_n under complex biological conditions.

The absorption and emission spectra of both NIR-CPS and NIR-CHO in different solvents (PBS/DMSO (v/v 99 : 1), DMSO and acetonitrile) are also obtained. As anticipated, NIR-COH showed very faint fluorescence emission, and NIR-COH

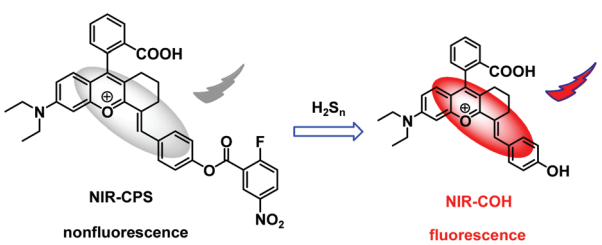

Scheme 1 Proposed response mechanism of NIR-CPS for H_2S_n.

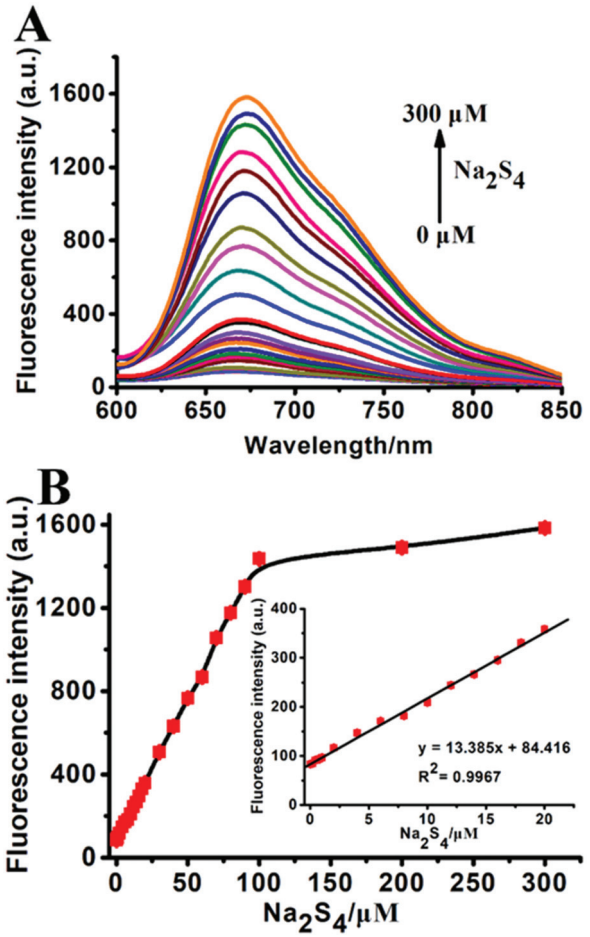

Fig. 1 Fluorescence response of NIR-CPS to H_2S_n. (A) Fluorescence spectra of NIR-CPS (10 μM) with Na_2S_4 (0, 0.5, 1, 2, 4, 6, 8, 10, 15, 20, 25, 30, 35, 40, 60, 80, 100, 200 and 300 μM) in PBS buffer (20 mM, pH = 7.4, 1% DMSO, containing 1 mM CTAB) at 37 °C for 30 min. (B) The fluorescence intensity changes of NIR-CPS (10 μM) at 670 nm after incubation with different concentrations of Na_2S_4 (0–300 μM). Inset: The linear relationship between the fluorescence intensity and the concentrations of Na_2S_4 (0–20 μM) in PBS buffer. Data are presented as the mean ± SD (n = 3).

showed maximum emission peaks around 670 nm–675 nm in different solvents (Fig. S2†). The fluorescence quantum yield of NIR-CHO is approximately 12.5% (in DMSO) and 12.8% (in acetonitrile); ICG in DMSO (Φ_f = 0.13) was used as a fluorescence standard. As shown in Fig. S3,† NIR-CPS has almost the same absorption spectra in different solvents. Additionally, NIR-COH also has the same absorption spectra in different solvents.

The reaction time of the probe with Na_2S_4 was further explored. As illustrated in Fig. S4,† the fluorescence response to Na_2S_4 reached saturation within approximately 20 min, and the fluorescence intensity did not change over 60 min, showing good stability of NIR-CPS.

The pH effects on the response of NIR-CPS and its response towards Na_2S_4 were also investigated. From pH 4.0 to 8.0, the fluorescence intensities gradually decreased, and the fluorescence was almost quenched at pH 9.0 (Fig. S5†). The observed fluorescence profile of NIR-CPS towards Na_2S_4 under different pH conditions is mainly due to the pH dependence of the emission profiles of NIR-COH.[51] There is an equilibrium between the phenolic and phenolate form in NIR-COH.[50]

As shown in Fig. S6,† the free probe showed negligible fluorescent signal. Within 60 min, the very faint emission intensity of the free probe did not change, showing good stability of NIR-CPS.

Selectivity of NIR-CPS for H_2S_n *in vitro*

To evaluate the selectivity of NIR-CPS towards H_2S_n, fluorescence responses were measured in the presence of various biological substances. As shown in Fig. 2, only Na_2S_2 and Na_2S_4 exhibited a dramatic fluorescence enhancement. However, other RSS, such as Na_2S, Cys, GSH, CysSSCys, Hcy, GSSG, S_8, $S_2O_3^{2-}$, SO_3^{2-}, SO_4^{2-}, Cys-polysulfide, and CH_3SSSCH_3, did not elicit any fluorescence enhancement. The NIR-CPS probe was not responsive to reactive oxygen species (H_2O_2, OCl^-, $^{\bullet}OH$, *t*BuOOH, $^1O_2$, O^{2-}) or reactive nitrogen species (NO_2^-, $ONOO^-$, NO, NO_3^-) (Fig. S7†). Various ions, such as Na^-, K^+, Cu^{2+}, Mg^{2+}, Zn^{2+}, Fe^{3+}, Fe^{2+}, CO_3^{2-}, HCO_3^-, Cl^-, Br^-, I^-, HPO_4^{2-}, and $H_2PO_4^-$, could not trigger interference (Fig. S8†). In addition, when Na_2S_2 (20 μM) and various other species coexisted, there was no obvious interference with fluorescence responses (Fig. 2, S7 and S8†). These results clearly indicate that NIR-CPS showed high selectivity to recognize H_2S_n over other biological species.

Fluorescence imaging of H_2S_n in living cells

Next, we exploited the capability of NIR-CPS to detect H_2S_n in living cells. Prior to cell imaging, standard MTT assays were performed to investigate the cytotoxicity of the probe. MCF-7 cells were selected as the test model for cell fluorescence imaging. When incubated with different concentrations of NIR-CPS (5 μM, 10 μM, 15 μM, 20 μM), the cell viability was higher than 90% (Fig. S9†). As shown in Fig. S10,† the cell viability showed almost no significant change over different incubation times (6 h, 12 h, 18 h, 24 h, 48 h). These results indicate that NIR-CPS has low cytotoxicity to MCF-7 cells at a concentration of 10 μM.

The untreated MCF-7 cells showed almost no fluorescence (Fig. 3). Cells treated with the free NIR-CPS probe (10 μM) exhibited relatively weak fluorescence emission (Fig. 3). To confirm the source of the weak fluorescence, the cells were pretreated with NMM (an efficient eliminator of H_2S_n,[40] 1 mM) for 1 h to remove the physiological levels of H_2S_n. Compared with the untreated cells, a significant decrease in the fluorescence intensity was observed in the NMM-treated cells, indicating that the NIR-CPS fluorescence change in the cells arises from the physiological levels of H_2S_n (Fig. 3). Then, treatment of probe-pretreated cells with different concentrations of Na_2S_4 (10 and 20 μM) led to a remarkable increase in the fluorescence emission (Fig. 3). Notably, the fluorescence intensities in these cells were further quantified, and the data indicate that the fluorescence induced by exogenous H_2S_n was con-

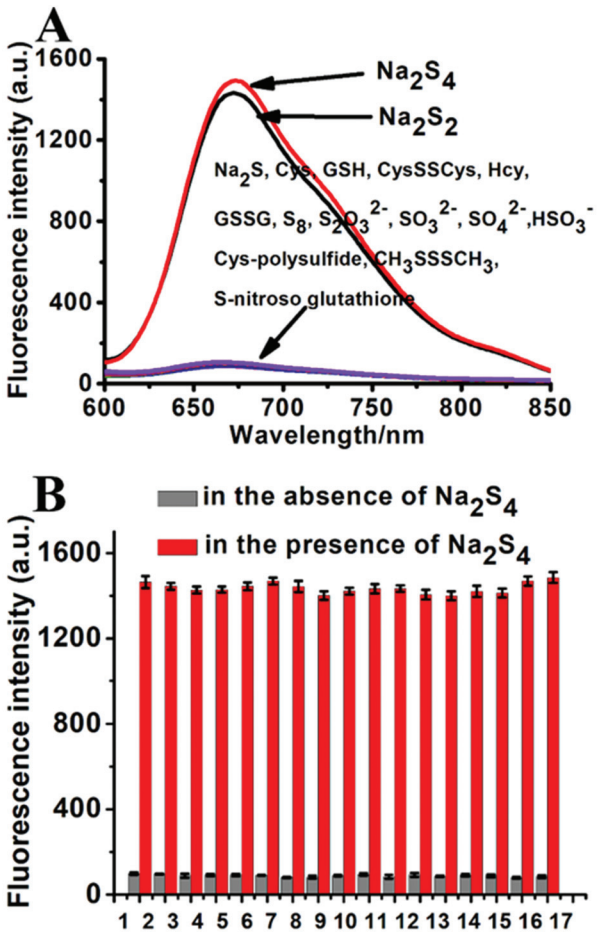

Fig. 2 The selectivity of NIR-CPS for H_2S_n. (A) Fluorescence spectra of NIR-CPS (10 μM) towards Na_2S_4 (100 μM), Na_2S_2 (100 μM) and various reactive sulfur species (20 μM Na_2S; 1 mM Cys; 1 mM GSH; 1 mM CysSSCys; 100 μM Hcy; 10 mM GSH; 1 mM GSSG; 500 μM S_8; 500 μM $Na_2S_2O_3$; 500 μM Na_2SO_3; 500 μM $NaHSO_3$; 500 μM Na_2SO_4; 1 mM Cys-polysulfide; 100 μM CH_3SSSCH_3; 1 mM *S*-nitroso glutathione) in PBS buffer (20 mM, pH = 7.4, 1% DMSO, containing 1 mM CTAB) at 37 °C for 30 min. (B) Fluorescence responses of NIR-CPS (10 μM) towards Na_2S_4 (100 μM), Na_2S_2 (100 μM) and various reactive sulfur species at 37 °C for 30 min. In each group, the red bars represent the relative responses at 670 nm of NIR-CPS to RSS and the mixture of RSS with 100 μM Na_2S_4. 1. Na_2S_4 (100 μM); 2. Na_2S_2 (100 μM); 3. Na_2S (20 μM); 4. Cys (1 mM); 5. GSH (1 mM); 6. CysSSCys (1 mM); 7. Hcy (100 μM); 8. GSH (10 mM); 9. GSSG (1 mM); 10. S_8 (500 μM); 11. $Na_2S_2O_3$ (500 μM); 12. Na_2SO_3 (500 μM); 13. Na_2SO_4 (500 μM); 14. Cys-poly sulfide (1 mM); 15. CH_3SSSCH_3 (100 μM); 16. $NaHSO_3$ (500 μM); 17. *S*-nitrosoglutathione (1 mM). Data are presented as the mean ± SD (n = 3).

centration dependent (4-fold, 5.6-fold). These results imply that NIR-CPS is capable of monitoring varying concentrations of exogenous and physiological H_2S_n inside living cells.

Having demonstrated the capability of NIR-CPS to monitor exogenous H_2S_n in cells, we further validated the capability of NIR-CPS to visualize endogenously produced H_2S_n in MCF-7 cells. Cystathionine γ-lyase (CSE) is regarded as the major enzyme for H_2S_n generation.[52] Lipopolysaccharide (LPS, 1 μg mL^{-1}) can upregulate CSE expression, resulting in an increase in endogenous H_2S_n levels in cells.[53] Therefore, LPS can

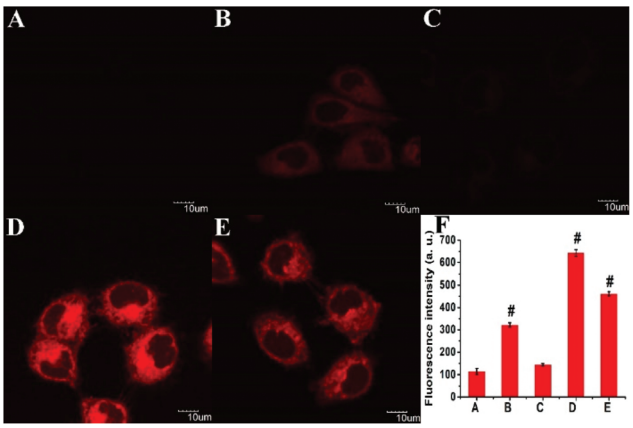

Fig. 3 Confocal fluorescence imaging of exogenous H_2S_n in living MCF-7 cells using NIR-CPS. Cells were untreated (A) or incubated (B) with NIR-CPS (10 μM) for 20 min at 37 °C. Cells were pretreated with *N*-ethylmaleimide (NMM, 1 mM) for 1 h, and then incubated with NIR-CPS (10 μM) for 20 min (C). Cells were incubated with NIR-CPS (10 μM) for 20 min and then further incubated with Na_2S_4 (20 μM) for 20 min (D). Cells were incubated with NIR-CPS (10 μM) for 20 min and then further incubated with Na_2S_4 (10 μM) for 20 min (E). The average fluorescence intensity of the above images (F). Scale bars = 10 μm. Data are presented as the mean ± SD (n = 3). $^{\#}p < 0.001$ *vs.* (A) column.

induce the production of endogenous H_2S_n in cells. After the addition of NIR-CPS to the culture of the LPS-loaded cells, the fluorescence signal dramatically increased (2.8-fold, Fig. 4). However, the cells were pretreated with PAG (CSE inhibitor, DL-propargylglycine) and subsequently incubated with LPS and the NIR-CPS probe. A remarkable decrease in fluorescence intensity was observed, suggesting that the fluorescence signal in Fig. 4 was caused by H_2S_n through LPS stimulation. These results revealed the capability of NIR-CPS to image endogenously produced H_2S_n in living cells.

Fluorescence imaging of H_2S_n *in vivo*

The excellent features of NIR-CPS, including NIR emission, high sensitivity and good selectivity, make the probe more favourable for fluorescence imaging of H_2S_n *in vivo*. Inspired

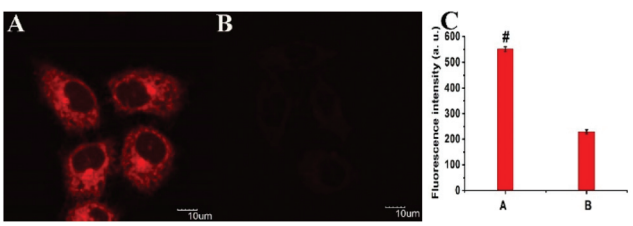

Fig. 4 Confocal fluorescence imaging of endogenous H_2S_n in living MCF-7 cells using NIR-CPS. The cells were induced by LPS (1 μg mL^{-1}) for 16 h, and then incubated with NIR-CPS (10 μM) for 20 min (A). Cells were preincubated with DL-propargylglycine (PAG, 200 μM) for 30 min and further treated with LPS (1 μg mL^{-1}) for 16 h at 37 °C. Then the cells were incubated with NIR-CPS (10 μM) for 20 min (B). The average fluorescence intensity of the above images (C). Scale bars = 10 μm. Data are presented as the mean ± SD (n = 3). $^{\#}p < 0.001$ *vs.* (B) column.

by the advantages of NIR-CPS, we further investigated the capability of the probe to visualize H_2S_n in living mice. Mice were divided into several groups. One group was i.p. injected with the free probe as the control group. The other three groups were i.p. injected with the NIR-CPS probe, followed by i.p. injection with various amounts of Na_2S_4 (0.2, 2.0 and 4.0 equiv.). The other group was injected with LPS and then injected with the free probe after 24 h. The last group was pretreated with DL-propargylglycine for 30 min and then i.p. injected with LPS for 24 h followed by a subsequent i.p. injection of NIR-CPS. Fluorescence signals from the whole-body area of the mice were imaged and quantified using a Night OWL IILB 983 small animal *in vivo* imaging system. The mice in the control group exhibited almost no fluorescence (Fig. 5). However, compared with the control group, the mice treated with both Na_2S_4 (0.2, 2.0 and 4.0 equiv.) and the probe displayed a marked elevation in the fluorescence intensities (3.2-, 6.5-, and 10.2-fold), indicating that our probe shows the desirable penetration for imaging exogenous H_2S_n *in vivo* (Fig. 5). Moreover, the mice injected with LPS and the probe also showed increased fluorescence emission (5.5-fold) (Fig. 5). With the i.p. injection of LPS into PAG-pretreated mice, the fluorescence of the mice was remarkably weakened (Fig. 5), indicating that a strong fluorescence was triggered by endogenous H_2S_n induced by LPS.

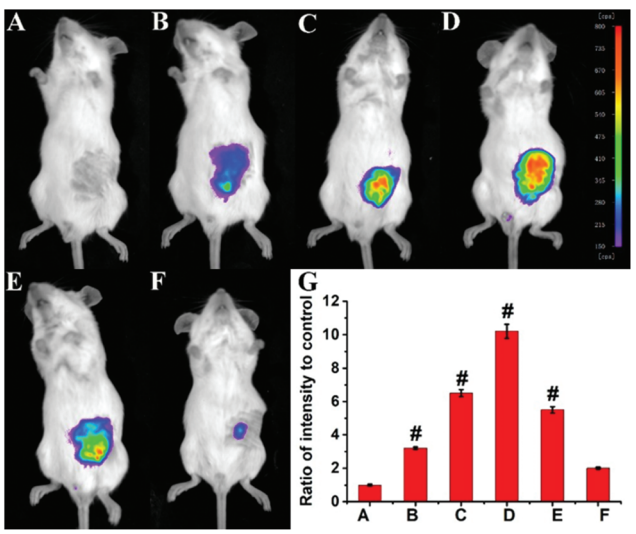

Fig. 5 Representative fluorescence images visualizing exogenous and endogenous H_2S_n in living mice using NIR-CPS. The mice were i.p. injected with the NIR-CPS probe (2 mM, 100 μL DMSO) as the control group (A). The mice were i.p. injected with the NIR-CPS probe (2 mM, 100 μL DMSO) for 15 min, followed by i.p. injection of 0.2 equiv. of Na_2S_4 (0.4 mM, 100 μL saline) (B). The mice were i.p. injected with the NIR-CPS probe (2 mM, 100 μL DMSO) for 15 min, followed by i.p. injection of 2 equiv. of Na_2S_4 (4 mM, 100 μL saline) (C). The mice were i.p. injected with the NIR-CPS probe (2 mM, 100 μL DMSO) for 15 min, followed by i.p. injection of 4 equiv. of Na_2S_4 (8 mM, 100 μL saline) (D). The mice were i.p. injected with LPS (10 μg mL^{-1}, 100 μL in 1 : 9 DMSO/saline v/v) for 24 h, followed by i.p. injection of NIR-CPS (2 mM, 100 μL DMSO) (E). The mice were pretreated (i.p. injection) with DL-propargylglycine (2 mM, 100 μL in saline) for 30 min, then i.p. injected with LPS (10 μg mL^{-1}, 100 μL in 1 : 9 DMSO/saline v/v) for 24 h, and a subsequent i.p. injection of NIR-CPS (2 mM, 100 μL DMSO) (F). Quantification of the relative fluorescence intensities from the abdominal area of the mice in the above groups (G). Images were taken after incubation for 25 min. Data are presented as the mean ± SD (n = 3). $^{\#}P < 0.001$ *vs.* Group A.

Next, the fluorescence intensities of the whole mice were detected in real time within 40 min after i.p. injection of the NIR-CPS probe. As illustrated in Fig. S13,† obvious fluorescence was observed within 1 min, and the maximum fluorescence intensity of the mice was obtained at approximately 25 min, and the intensity was maintained for 40 min. The data show that NIR-CPS had a fast response to H_2S_n, and the fluorescence intensities *in vivo* were stable. All these data establish that NIR-CPS is sensitive enough to monitor various levels of H_2S_n and is suitable for long-term monitoring of H_2S_n in living animals.

Bioluminescence imaging of H_2S_n in tumour-bearing mice

The imbalance between ROS generation and cellular antioxidant capacity is an important pathogenic factor in several diseases, such as tumours.[53] Reactive sulfur species (RSS) have a crucial function in regulating the intracellular redox state.[2,54] Specifically, H_2S_n displays strong reducing and nucleophilic abilities and is associated with scavenging oxidants and intracellular electrophiles.[16,55–58] The levels of H_2S_n *in vivo* might be involved in the pathogenesis of tumours.[41] In addition, several inorganic polysulfide donors (Na_2S_2 and Na_2S_4) and garlic-derived organic polysulfide also exhibited anticancer activities.[59–61] Nevertheless, the underlying mechanisms of the anticancer effects of H_2S_n are not clear. Therefore, probes that can monitor level changes of H_2S_n in tumours are critical for further elucidating the physiological and pathological role of H_2S_n in tumours.

We next sought to investigate the feasibility of the NIR-CPS probe for imaging H_2S_n in tumour-bearing mice. MCF-7 cells were grafted into nude mice to produce murine xenograft tumour models. The nude mice were divided into several groups. The mice were intravenously injected with NIR-CPS alone as the control group. One group was intratumourally injected with LPS for 24 h and then intravenously injected with the NIR-CPS probe. The other mice were intratumourally injected with DL-propargylglycine for 30 min and then intratumourally injected with LPS for 24 h, followed by a subsequent intravenous injection of NIR-CPS. The fluorescence signals from the tumours in the nude mice were imaged and quantified. Fig. 6 shows almost no fluorescence emission in the probe-loaded group. After the intratumoural injection of LPS into the nude mice, the fluorescence intensities in the tumours remarkably increased (27.5-fold, Fig. 6). However, the fluorescence in the nude mice pretreated with DL-propargylglycine decreased dramatically, indicating that the fluorescence in the tumour was triggered by LPS-induced endogenous H_2S_n (Fig. 6). Subsequently, the fluorescence intensities were quantified in real time within 50 min after intravenous injection of the NIR-CPS probe. A significant fluorescence signal could be detected within the first 5 min, indicating the fast response of

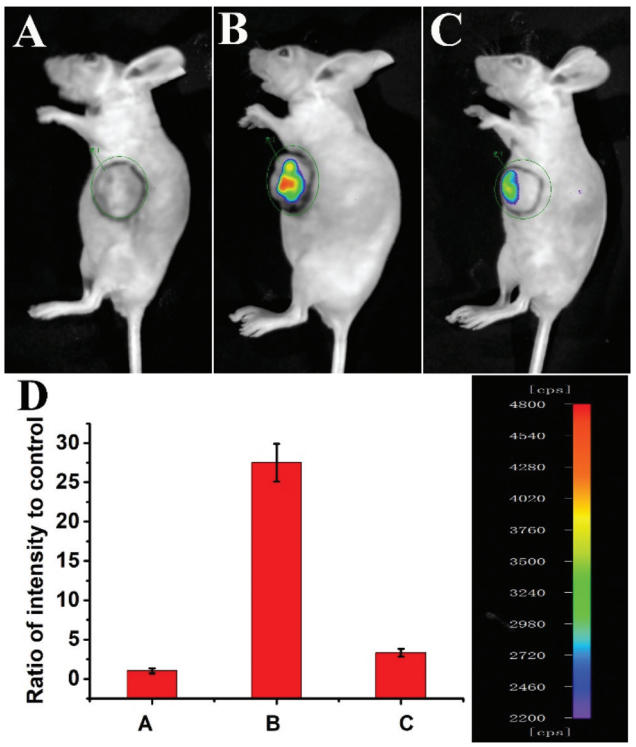

Fig. 6 Representative fluorescence images of NIR-CPS in tumour-bearing mice. (A) Mice were intravenously injected with NIR-CPS (2 mM, 100 μL saline, 3% DMSO, 1% Tween 80) as the control group. (B) Mice were intratumourally injected with LPS (10 μg mL^{-1}, 100 μL in saline) for 24 h, followed by intravenous injection of NIR-CPS (2 mM, 100 μL saline, 3% DMSO, 1% Tween 80). (C) The mice were pretreated (intratumoural injection) with DL-propargylglycine (2 mM, 100 μL in saline) for 30 min and then intratumourally injected with LPS (10 μg mL^{-1}, 100 μL in 1 : 9 DMSO/saline v/v) for 24 h, followed by intravenous injection of NIR-CPS (2 mM, 100 μL DMSO). (D) Quantification of the fluorescence intensity from the tumour area of mice from all groups. Data are presented as the mean ± SD (n = 3).

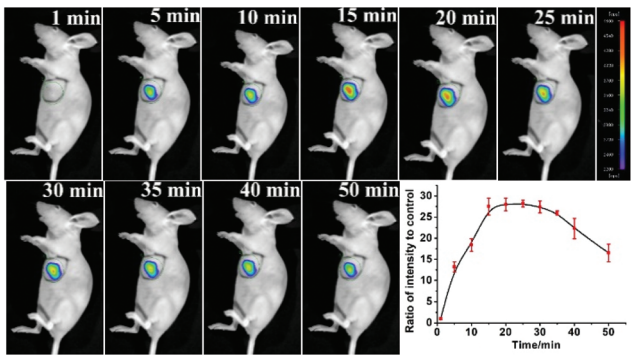

Fig. 7 Representative fluorescence images of visualizing the H_2S_n levels at different times in tumour-bearing mice using NIR-CPS. Mice were intratumourally injected with LPS (10 μg mL^{-1}, 100 μL in saline) for 24 h, followed by intravenous injection of NIR-CPS (2 mM, 100 μL saline, 3% DMSO, 1% Tween 80). Images were taken after incubation with LPS for 1 min, 5 min, 10 min, 15 min, 20 min, 25 min, 30 min, 35 min, 40 min, and 50 min. Quantification of the fluorescence intensity from the tumour area of mice from all groups. Data are presented as the mean ± SD (n = 3).

NIR-CPS towards H_2S_n in the tumour. Moreover, the fluorescence intensities in the tumour region reached their peak value at 15 min (28-fold) and gradually decreased after 40 min (Fig. 7). These results suggest that our probe could detect H_2S_n level changes in tumours.

Conclusions

To conclude, we developed a novel fluorescence probe that showed a remarkably large Stokes shift, high sensitivity, and ideal selectivity towards H_2S_n. This probe was successfully applied for the selective imaging of endogenous H_2S_n induced by LPS in living cells and mice. Notably, fluorescence imaging of H_2S_n in nude mice bearing MCF-7 tumours indicated that the fluctuations of H_2S_n in cancerous tissues could be selectively monitored by our probe. We anticipate that this new probe will show great potential as an effective tool in the exploration of H_2S_n-related roles in tumours.

Experimental

Synthesis of NIR-CPS

Compound 1 (0.2 g, 0.53 mmol),[49–51] compound 2 (0.23 g, 0.80 mmol) and piperidine (5.2 μL, 0.05 mmol) were dissolved in dry ethanol (15 mL). The mixture was refluxed for 6 h. The solvent was removed under reduced pressure, and then, the crude product was dissolved in 100 mL of dichloromethane and washed with 30 mL of water. The organic layers were dehydrated with Na_2SO_4, and then the solvent was evaporated. The crude product was purified using a silica gel column to produce compound NIR-CPS as a purple solid (50 mg, 14.5%). TLC (silica, CH_2Cl_2 : CH_3OH, 10 : 1 v/v): R_f = 0.40; ^{1}H NMR (400 MHz, $CDCl_3$): δ 9.03 (dd, J = 5.6, 2.8 Hz, 1H), 8.48–8.52 (m, 1H), 7.96 (d, J = 7.6 Hz, 1H), 7.65 (t, J = 7.2 Hz, 1H), 7.56 (t, J = 7.6 Hz, 1H), 7.40–7.48 (m, 4H), 7.23–7.25 (m, 1H), 7.28 (s, 1H), 6.35–6.51 (m, 3H), 3.36 (q, J = 6.8 Hz, J = 14.0 Hz, 4H), 2.64–2.83 (m, 2H), 2.05–2.09 (m, 2H), 1.60–1.70 (m, 2H), 1.18 (t, J = 7.2 Hz, 6H); ^{13}C NMR (100 MHz, $CDCl_3$): δ 170.14, 168.86, 164.15, 160.72, 152.59, 152.29, 149.41, 148.96, 146.83, 144.05, 135.80, 134.60, 131.30, 130.76, 130.35, 130.25, 129.36, 128.66, 127.64, 125.06, 124.10, 123.58, 121.22, 118.964, 118.72, 108.84, 108.41, 104.80, 97.31, 44.52, 27.24, 23.11, 22.48, 12.65. HRMS (ESI^+): $(M)^+$ calcd for $C_{38}H_{32}FN_2O_7$, 647.2118; found, 647.2190.

Fluorometric analysis *in vitro*

All fluorescence measurements were accomplished on a Hitachi F4600 Fluorescence Spectrophotometer. Na_2S_4 (or Na_2S_2) was used as the H_2S_n source in all experiments. The NIR-CPS probe solution (DMSO) was placed in a quartz cuvette. With the probe diluted to 10 μM with 20 mM PBS buffer, various amounts of Na_2S_4 were added. The resulting solution was then incubated for 30 min, and fluorescence spectra were obtained with an excitation wavelength of 570 nm. The emission spectra were collected from 600 nm to 850 nm at a velocity of 1200 nm min^{-1}.

A photomultiplier voltage of 1000 V was used. Data are presented as the mean ± SD (n = 3).

Fluorescence imaging of living cells

The MCF-7 cells were treated with 10% (v/v) FBS (foetal bovine serum) and penicillin/streptomycin (100 μg mL^{-1}) at 37 °C in a 5% CO_2 incubator. Cells were permitted to grow to 80% confluence before harvesting and were seeded in a glass-bottom plate. NIR-CPS solution (the final concentration of 10 μM, 1.0 mM stock solution in DMSO) was added to the cell media and incubated under the previous conditions for 20 min. For exogenous H_2S_n imaging, the probe-treated cells were then further incubated with Na_2S_4 (1.0 mM stock solution in DI H_2O, the final concentration of 10 μM or 20 μM) for 20 min. For endogenous H_2S_n imaging, the cells were pretreated with LPS (1 μg mL^{-1}) for 16 h and then incubated with NIR-CPS (the final concentration of 10 μM) for 20 min. All cells were rinsed thrice with PBS buffer prior to imaging. Confocal fluorescence imaging was performed on an Olympus FV1000 confocal laser scanning microscope with 60× oil objectives. The excitation wavelength was 570 nm. The fluorescence images (670 nm) were obtained at 1024 × 1024 pixels and were analysed with Olympus software (FV10-ASW). All data are expressed as the mean ± SD (n = 3).

Animals and administration

All animal experiments were carried out in compliance with the Chinese legislation on the use and care of laboratory animals and were approved by the Institutional Animal Care and Use Committee of Xuzhou Medical University. Adult male Kunming mice weighing 20–25 g were provided by the Experimental Animal Centre of Xuzhou Medical College. Female nude mice weighing 20–25 g (six to eight weeks old) were purchased from Shanghai Sippr-BK Laboratory Animal Co., Ltd. All mice were housed in a room with regulated temperature (22 ± 2 °C) and humidity (50 ± 10%) on a 12 h light/dark cycle. The animals had *ad libitum* access to standard commercial animal feed and pure water, and were maintained under specific pathogen-free conditions. Mice were acclimatized for 1 week prior to experiments.

Fluorescence imaging of living mice

Prior to *in vivo* imaging, the mice were anaesthetized by i.p. injection of 10% chloral hydrate (0.04 mL per 10 g), and their abdominal fur was removed. The mice were randomly selected and divided into several groups. The mice were given i.p. injection of the free NIR-CPS probe (2 mM, 100 μL DMSO) as the control group. For exogenous H_2S_n imaging, the other three groups were i.p. injected with the NIR-CPS probe (2 mM, 100 μL DMSO) for 15 min, followed by i.p. injection of 0.2 equiv. of Na_2S_4 (0.4 mM, 100 μL saline), 2 equiv. of Na_2S_4 (4 mM, 100 μL saline), or 4 equiv. of Na_2S_4 (8 mM, 100 μL saline). For endogenous H_2S_n imaging stimulated by LPS, the other groups were i.p. injected with LPS (10 μg mL^{-1}, 100 μL in 1 : 9 DMSO/saline v/v) for 24 h, followed by i.p. injection of NIR-CPS (2 mM, 100 μL DMSO). The last group was pretreated (i.p. injection) with DL-propargylglycine (2 mM, 100 μL in saline) for 30 min, then i.p. injected with LPS (10 μg mL^{-1}, 100 μL in 1 : 9 DMSO/saline v/v) for 24 h and given a subsequent i.p. injection of NIR-CPS (2 mM, 100 μL DMSO). For the time-dependent experiment, the mice were i.p. injected with LPS (10 μg mL^{-1}, 100 μL in saline) for 24 h, followed by i.p. injection of NIR-CPS (2 mM, 100 μL DMSO). The fluorescence intensities were then recorded after incubation of NIR-CPS at different times (0 min; 1 min; 5 min; 10 min; 15 min; 20 min; 25 min; 30 min; 35 min; 40 min). The mice were imaged using a Night OWL IILB 983 small animal *in vivo* imaging system, with an excitation filter of 485 nm and an emission filter of 680 nm. The fluorescence signals were quantified with Olympus software (FV10-ASW). All data are expressed as the mean ± SD (n = 3).

Fluorescence imaging in tumour-bearing mice

Female BALB/c nude mice received a subcutaneous injection of 10^7 MCF-7 tumour cells. Tumours with a volume of approximately 200 mm^3 were formed over a period of 4 weeks. Mice bearing implanted tumours were anaesthetized by i.p. injection of 10% chloral hydrate (0.04 mL per 10 g) and then randomly divided into several groups. Mice were intravenously injected with NIR-CPS (2 mM, 100 μL saline, 3% DMSO, 1% Tween 80) as the control group. The experimental group was intratumourally injected with LPS (10 μg mL^{-1}, 100 μL in saline) for 24 h, followed by intravenous injection of NIR-CPS (2 mM, 100 μL saline, 3% DMSO, 1% Tween 80). The other mice were pretreated (intratumoural injection) with DL-propargylglycine (2 mM, 100 μL in saline) for 30 min, then intratumourally injected with LPS (10 μg mL^{-1}, 100 μL in saline) for 24 h and given a subsequent intravenous injection of NIR-CPS (2 mM, 100 μL saline, 3% DMSO, 1% Tween 80). After injection of the NIR-CPS probe, fluorescence images were obtained at a series of time points within 40 min (0 min; 1 min; 5 min; 10 min; 15 min; 20 min; 25 min; 30 min; 35 min; 40 min) using a Night OWL IILB 983 small animal *in vivo* imaging system with an excitation filter of 485 nm and an emission filter of 680 nm. All data are expressed as the mean ± SD (n = 3).

Statistical analyses

All statistical analyses were performed using SPSS software, version 16.0 (SPSS Inc., Chicago, IL, USA). Values are reported as the mean ± SD (standard deviation of the mean). The data were analysed with one-way analysis of variance (ANOVA). Statistical significance was set at $p < 0.05$.

Conflicts of interest

There are no conflicts to declare.

Acknowledgements

This project was financed by the Open Program of NHC Key Laboratory of Nuclear Medicine and Jiangsu Key Laboratory of

Molecular Nuclear Medicine (KF201906) and the Postgraduate Research & Practice Innovation Program of Jiangsu Province (SJCX19_0947), Jiangsu Overseas Visiting Scholar Program for University Prominent Young & Middle-aged Teachers and Presidents, and the Science and Technology Project of Xuzhou (KC19044, KC18048). The authors also acknowledge the support for this work from the Priority Academic Programme Development of Jiangsu Higher Education Institutions (PAPD).

Notes and references

1 I. Giles, K. M. Tasker and C. Jacob, *Free Radicals Biol. Med.*, 2001, **31**, 1279–1283.
2 M. C. Gruhlke and A. J. Slusarenko, *Plant Physiol. Biochem.*, 2012, **59**, 98–107.
3 G. I. Giles and C. Jacob, *Biol. Chem.*, 2002, **383**, 375–388.
4 H. Liu, M. N. Radford, C. T. Yang, W. Chen and M. Xian, *Br. J. Pharmacol.*, 2019, **176**, 616–627.
5 O. Kabil and R. Banerjee, *J. Biol. Chem.*, 2010, **285**, 21903–21907.
6 H. Kimura, *Antioxid. Redox Signal.*, 2014, **20**, 783–793.
7 C. Szabo, R. Céline, M. Katalin, M. Andriamihaja, B. Murghes, C. Coletta, G. Olah, K. Yanagi and F. Bouillaud, *Br. J. Pharmacol.*, 2014, **171**, 2099–2122.
8 M. Katalin, M. B. Eelke, C. Enrico, G. Harry van, C. Ciro, P. Andreas, R. H. Mark, R. Peter, B. Frédéric and S. Csaba, *Br. J. Pharmacol.*, 2014, **171**, 2123–2146.
9 P. Nagy and C. C. Winterbourn, *Chem. Res. Toxicol.*, 2010, **23**, 1541–1543.
10 K. M. Miranda and D. A. Wink, *Proc. Natl. Acad. Sci. U. S. A.*, 2014, **111**, 7505–7506.
11 H. Kimura, *Antioxid. Redox Signal.*, 2015, **22**, 362–376.
12 T. V. Mishanina, M. Libiad and R. Banerjee, *Nat. Chem. Biol.*, 2015, **11**, 457–464.
13 H. Kimura, *Proc. Jpn. Acad., Ser. B, Phys. Biol. Sci.*, 2015, **91**, 131–159.
14 R. Greiner, Z. Pálinkás, K. Bäsell, D. Becher, H. Antelmann, P. Nagy and T. P. Dick, *Antioxid. Redox Signal.*, 2013, **19**, 1749–1765.
15 P. K. Yadav, M. Martinov, V. Vitvitsky, J. Seravalli, R. Wedmann, M. R. Filipovic and R. Banerjee, *J. Am. Chem. Soc.*, 2016, **138**, 289–299.
16 K. Ono, T. Akaike, T. Sawa, Y. Kumagai, D. A. Wink, D. J. Tantillo, A. J. Hobbs, P. Nagy, M. Xian, J. Lin and J. M. Fukuto, *Free Radicals Biol. Med.*, 2014, **77**, 82–94.
17 B. B. Tao, S. Y. Liu, C. C. Zhang, W. Fu, W. J. Cai, Y. Wang, Q. Shen, M. J. Wang, Y. Chen, L. J. Zhang, Y. Z. Zhu and Y. C. Zhu, *Antioxid. Redox Signal.*, 2013, **19**, 448–464.
18 Y. Kimura, Y. Mikami, K. Osumi, M. Tsugane, J. Oka and H. Kimura, *FASEB J.*, 2013, **27**, 2451–2457.
19 Y. Hatakeyama, K. Takahashi, M. Tominaga, H. Kimura and T. Ohta, *Mol. Pain*, 2015, **11**, 24.
20 G. Pozsgai, I. Z. Bátai and E. Pintér, *Br. J. Pharmacol.*, 2019, **176**, 628–645.
21 D. Stubbert, O. Prysyazhna, O. Rudyk, J. Scotcher, J. R. Burgoyne and P. Eaton, *Hypertension*, 2014, **64**, 1344–1351.
22 S. Koike, Y. Ogasawara, N. Shibuya, H. Kimura and K. Ishii, *FEBS Lett.*, 2013, **587**, 3548–3555.
23 H. Kimura, *Neurochem. Int.*, 2019, **126**, 118–125.
24 S. Koike, K. Kawamura, Y. Kimura, N. Shibuya, H. Kimura and Y. Ogasawara, *Free Radicals Biol. Med.*, 2017, **113**, 355–362.
25 (*a*) J. Zhou and H. Ma, Design principles of spectroscopic probes for biological applications, *Chem. Sci.*, 2016, **7**, 6309–6315; (*b*) J. Zheng, S. Feng, S. Gong, Q. Xia and G. Feng, *Sens. Actuators, B*, 2020, **309**, 127796; (*c*) X. Yin, W. Feng, S. Gong and G. Feng, *Dyes Pigm.*, 2020, **172**, 107820.
26 (*a*) X. Chen, F. Wang, J. Y. Hyun, T. Wei, J. Qiang, X. Ren, I. Shin and J. Yoon, *Chem. Soc. Rev.*, 2016, **45**, 2976–3016; (*b*) S. Gong, E. Zhou, J. Hong and G. Feng, *Anal. Chem.*, 2019, **91**, 13136–13142; (*c*) E. Zhou, S. Gong and G. Feng, *Sens. Actuators, B*, 2019, **301**, 127075.
27 C. Liu, W. Chen, W. Shi, B. Peng, Y. Zhao, H. Ma and M. Xian, *J. Am. Chem. Soc.*, 2014, **136**, 7257–7260.
28 W. Meng, W. Shi, Y. Chen, H. Zhang, J. Zhao, Z. Li and K. Xiao, *Sens. Actuators, B*, 2019, **281**, 871–877.
29 Y. Huang, F. Yu, J. Wang and L. Chen, *Anal. Chem.*, 2016, **88**, 4122–4129.
30 J. Zhang, X. Y. Zhu, X. X. Hu, H. W. Liu, J. Li, L. L. Feng, X. Yin, X. B. Zhang and W. Tan, *Anal. Chem.*, 2016, **88**, 11892–11899.
31 J. Guo, S. Yang, C. Guo, Q. Zeng, Z. Qing, Z. Cao, J. Li and R. Yang, *Anal. Chem.*, 2018, **90**, 881–887.
32 F. Yu, M. Gao, M. Li and L. Chen, *Biomaterials*, 2015, **63**, 93–101.
33 W. Chen, A. Pacheco, Y. Takano, J. J. Day, K. Hanaoka and M. Xian, *Angew. Chem., Int. Ed.*, 2016, **55**, 9993–9996.
34 Q. Han, J. Ru, W. Wang, Z. Dong, L. Wang, H. Jiang and W. Liu, *ACS Appl. Bio Mater.*, 2019, **2**, 1987–1997.
35 J. B. Li, Q. Wang, H. W. Liu, L. Yuan and X. B. Zhang, *Chem. Commun.*, 2019, **55**, 4487–4490.
36 Y. Fang, W. Chen, W. Shi, H. Li, M. Xian and H. Ma, *Chem. Commun.*, 2017, **53**, 8759–8762.
37 Q. Han, Z. Mou, H. Wang, X. Tang, Z. Dong, L. Wang, X. Dong and W. Liu, *Anal. Chem.*, 2016, **88**, 7206–7212.
38 W. Chen, E. W. Rosser, T. Matsunaga, A. Pacheco, T. Akaike and M. Xian, *Angew. Chem., Int. Ed.*, 2015, **54**, 13961–13965.
39 J. Ma, J. Fan, H. Li, Q. Yao, F. Xu, J. Wang and X. Peng, *J. Mater. Chem. B*, 2017, **5**, 2574–2579.
40 L. Zeng, S. Chen, T. Xia, W. Hu, C. Li and Z. Liu, *Anal. Chem.*, 2015, **87**, 3004–3010.
41 M. Gao, X. Zhang, Y. Wang, Q. Liu, F. Yu, Y. Huang, C. Ding and L. Chen, *Anal. Chem.*, 2019, **91**, 7774–7781.
42 R. Kawagoe, I. Takashima, S. Uchinomiya and A. Ojida, *Chem. Sci.*, 2017, **8**, 1134–1140.
43 Y. Ren, L. Zhang, Z. Zhou, Y. Luo, S. Wang, S. Yuan, Y. Gu, Y. Xu and X. Zha, *Anal. Chim. Acta*, 2019, **1056**, 117–124.
44 H. Dong, Q. Zhou, L. Zhang and Y. Tian, *Angew. Chem., Int. Ed.*, 2019, **58**, 13948–13953.

45 H. Zhou, J. Tang, L. Sun, J. Zhang, B. Chen, J. Kana, W. Zhang, J. Zhang and J. Zhou, *Sens. Actuators, B*, 2019, **278**, 64–72.
46 H. J. Choia, C. S. Lima, M. K. Choa, J. S. Kanga, S. J. Park, S. M. Park and H. M. Kima, *Sens. Actuators, B*, 2019, **283**, 810–819.
47 Z. Guo, S. Park, J. Yoon and I. Shin, *Chem. Soc. Rev.*, 2014, **43**, 16–29.
48 L. Yuan, W. Lin, K. Zheng, L. He and W. Huang, *Chem. Soc. Rev.*, 2013, **42**, 622–661.
49 L. Yuan, W. Lin, Y. Yang and H. Chen, *J. Am. Chem. Soc.*, 2012, **134**, 1200–1211.
50 L. Yuan, W. Lin and H. Chen, *Biomaterials*, 2013, **34**, 9566–9571.
51 K. Liu, H. Shang, X. Kong, M. Ren, J. Y. Wang, Y. Liu and W. Lin, *Biomaterials*, 2016, **100**, 162–171.
52 T. Ida, T. Sawa, H. Ihara, Y. Tsuchiya, Y. Watanabe, Y. Kumagai, M. Suematsu, H. Motohashi, S. Fujii, T. Matsunaga, M. Yamamoto, K. Ono, N. O. Devarie-Baez, M. Xian, J. M. Fukuto and T. Akaike, *Proc. Natl. Acad. Sci. U. S. A.*, 2014, **111**, 7606–7611.
53 X. Y. Zhu, S. J. Liu, Y. J. Liu, S. Wang and X. Ni, *Cell. Mol. Life Sci.*, 2010, **67**, 1119–1132.
54 V. S. Lin, W. Chen, M. Xian and C. J. Chang, *Chem. Soc. Rev.*, 2015, **44**, 4596–4618.
55 J. M. Fukuto, L. J. Ignarro, P. Nagy, D. A. Wink, C. G. Kevil, M. Feelisch, M. M. Cortese-Krott, C. L. Bianco, Y. Kumagai, A. J. Hobbs, J. Lin, T. Ida and T. Akaike, *FEBS Lett.*, 2018, **592**, 2140–2152.
56 K. R. Olson, *Free Radicals Biol. Med.*, 2019, **140**, 74–83.
57 Y. Takano, H. Echizen and K. Hanaoka, *Antioxid. Redox Signal.*, 2017, **27**, 669–683.
58 C. M. Park, L. Weerasinghe, J. J. Day, J. M. Fukuto and M. Xian, *Mol. BioSyst.*, 2015, **11**, 1775–1785.
59 N. E. B. Saidu, S. Valente, E. Ana, G. Kirsch, D. Bagrel and M. Montenarh, *Bioorg. Med. Chem.*, 2012, **20**, 1584–1593.
60 X. Cao, X. Nie, S. Xiong, L. Cao, Z. Wu, P. K. Moore and J. S. Bian, *Redox Biol.*, 2018, **15**, 513–521.
61 S. Miltonprabu, N. Sumedha and P. Senthilraja, *Int. Immunopharmacol.*, 2017, **50**, 107–120.